

---

# BUBBLEML: A MULTI-PHYSICS DATASET AND BENCHMARKS FOR MACHINE LEARNING

---

**Sheikh Md Shakeel Hassan**

Electrical Engineering and Computer Science  
University of California Irvine  
Irvine, CA 92617  
sheikhh1@uci.edu

**Arthur Feeney**

Electrical Engineering and Computer Science  
University of California Irvine  
Irvine, CA 92617  
afeeney@uci.edu

**Akash Dhruv**

Argonne National Laboratory  
Lemont, IL 60439  
adhruv@anl.gov

**Youngjoon Suh**

Mechanical and Aerospace Engineering  
University of California Irvine  
Irvine, CA 92617  
ysuh2@uci.edu

**Jihoon Kim**

Department of Mechanical Engineering  
Korea University, Seoul, 02841, Republic of Korea  
kimjihoon@korea.ac.kr

**Jaiyoung Ryu**

Department of Mechanical Engineering  
Korea University, Seoul, 02841, Republic of Korea  
jryu@korea.ac.kr

**Yoonjin Won**

Mechanical and Aerospace Engineering  
University of California Irvine  
Irvine, CA 92617  
won@uci.edu

**Aparna Chandramowlishwaran**

Electrical Engineering and Computer Science  
University of California Irvine  
Irvine, CA 92617  
amowli@uci.edu

July 28, 2023

**ABSTRACT**

In the field of phase change phenomena, the lack of accessible and diverse datasets suitable for machine learning (ML) training poses a significant challenge. Existing experimental datasets are often restricted, with limited availability and sparse ground truth data, impeding our understanding of this complex multi-physics phenomena. To bridge this gap, we present the BubbleML Dataset<sup>1</sup> which leverages physics-driven simulations to provide accurate ground truth information for various boiling scenarios, encompassing nucleate pool boiling, flow boiling, and sub-cooled boiling. This extensive dataset covers a wide range of parameters, including varying gravity conditions, flow rates, sub-cooling levels, and wall superheat, comprising 51 simulations. BubbleML is validated against experimental observations and trends, establishing it as an invaluable resource for ML research. Furthermore, we showcase its potential to facilitate exploration of diverse downstream tasks by introducing two benchmarks: (a) optical flow analysis to capture bubble dynamics, and (b) operator networks for learning temperature dynamics. The BubbleML dataset and its benchmarks serve as a catalyst for advancements in ML-driven research on multi-physics phase change phenomena, enabling the development and comparison of state-of-the-art techniques and models.

---

<sup>1</sup><https://github.com/HPCForge/BubbleML>

# 1 Introduction

Phase-change phenomena, such as boiling, involve complex multi-physics processes and dynamics that are not fully understood. The interplay between bubble dynamics and heat transfer performance during boiling presents significant challenges in accurately predicting and modeling these heat and mass transfer processes. Machine learning (ML) offers the potential to revolutionize this field, enabling data-driven discovery to unravel new physical insights [49], develop accurate surrogate and predictive models [48], optimize the design of heat transfer systems [25], and facilitate adaptive real-time monitoring and control [21].

The applications of ML in this domain are diverse and impactful. Consider the context of high-performance computing in data centers, where efficient cooling is critical. Boiling-based cooling techniques, such as two-phase liquid cooling, offer enhanced heat dissipation capabilities, ensuring reliable and optimal operation of power-intensive electronic components such as GPUs [33, 1]. Moreover, boiling phenomena play a crucial role in complex processes like nuclear fuel reprocessing, where precise modeling and prediction of boiling dynamics contribute to the safe and efficient management of nuclear waste [15]. In the realm of water desalination, boiling processes are integral, playing a vital role in thermal desalination methods that provide clean drinking water in water-scarce regions [19]. These advancements in pivotal areas such as thermal management, energy efficiency, and heat transfer applications, driven by ML techniques have far-reaching implications, empowering us to design more sustainable energy systems, enhance environmental preservation efforts, and advance engineering capabilities across various domains [22].

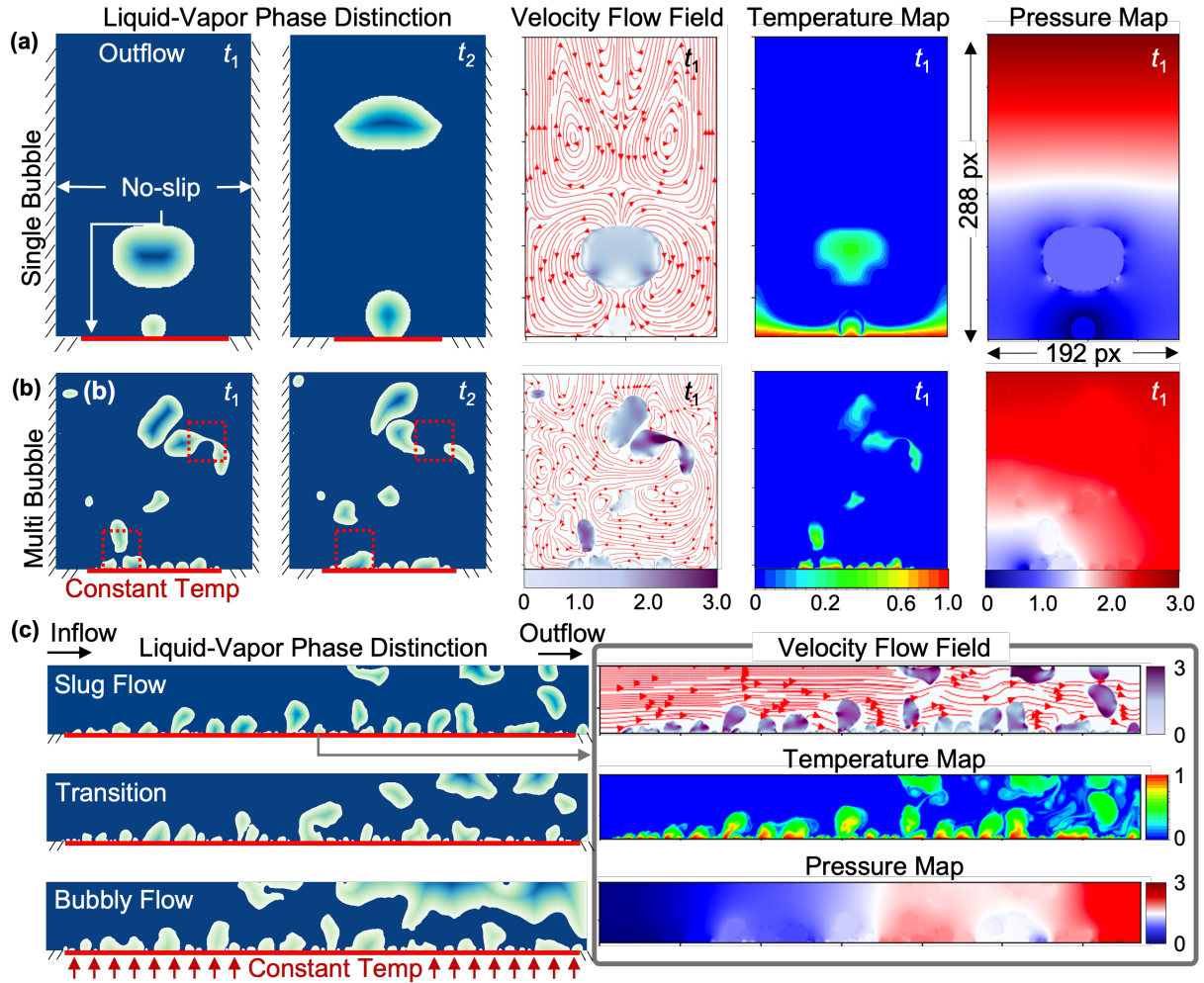


Figure 1: BubbleML: A comprehensive dataset of diverse two-phase boiling phenomena, providing ground truth for variables of physical importance, including velocity, temperature, and pressure, highlighting bubble and flow dynamics.

To train data-driven ML algorithms effectively, we need large, diverse, and accurately labeled datasets. However, obtaining high-fidelity datasets that encompass a wide range of phase-change phenomena and operating conditions is a significant challenge. Boiling processes are highly sensitive to factors like surface properties, pressure, orientation, and working fluid composition [2]. Additionally, the chaotic nature of vapor interactions and occlusions makes quantifying boiling processes inherently difficult [25]. Specialized experimental setups, involving instrumentation, sensors, and high-speed visualization techniques, come with substantial costs, further limiting the availability of extensive and accurate large-scale experimental data [48]. As a result, only a few well-funded research laboratories have access to precise ground truth data, and even then, this data often lacks fidelity and fails to capture detailed microscale dynamics, such as local bubble-induced turbulence and its impact on overall heat transfer. This scarcity of high-fidelity datasets poses challenges in designing accurate ML models for multiphase and phase change processes. While scientific ML (SciML) approaches can incorporate physical knowledge and constraints into the training process to reduce some of this data burden [37], the validation and quantification of uncertainty still rely on the availability of ground truth data. Therefore, there is an urgent need for open, diverse, and large-scale datasets to develop robust models and advance research in multi-physics problems such as phase change phenomena.

Simulations have played a key role as the third pillar of science in overcoming the inherent challenges faced by experimental studies in various scientific domains. High-fidelity multiscale data from simulations complement and enhance experimental measurements. In the field of phase change, simulations have successfully modeled transport equations for momentum, energy, and phase transition enabling accurate measurements of velocity, pressure, and temperature fields around bubbles [34, 41]. As a result, simulations serve as powerful tools for understanding and quantifying boiling. However, SciML researchers often setup their own simulations to generate ground truth solutions for training and testing their models, rather than relying on shared benchmark datasets. This is even common among major papers: [26, 30, 28]. While this approach is reasonable for studying specific, simple partial differential equations (PDEs), real-world applications of PDE solvers and simulations often involve large-scale systems with complex multiphase physics and a combination of Dirichlet and Neumann boundary conditions [47]. These real-world problems require substantial domain expertise, engineering time, and computational resources. Performing such simulations independently is impractical or even infeasible for many ML researchers. This difficulty in dataset generation has led to a drought of SciML research to study "real-world" physics problems. Previous efforts to build benchmark datasets have primarily focused on simpler problems with single-phase dynamics [50, 36].

As a response to the aforementioned challenges, we introduce the BubbleML Dataset <sup>2</sup>, an extensive and innovative collection of data generated through Flash-X simulations [13]. This dataset encompasses a wide range of boiling phenomena, including nucleate boiling of single bubbles, merging bubbles, flow boiling in different configurations, and subcooled boiling. Figure 1 provides a visual glimpse into the diverse range of physical phenomena and variables covered by the dataset. To further enhance its applicability, the dataset covers various gravity conditions ranging from earth gravity to gravity at the International Space Station, different heater temperatures and also different inlet velocities. In total, we present approximately 50 simulations, each capturing a specific combination of parameters and conditions. In summary, the key contributions are as follows:

**Multi-phase and Multi-physics Dataset.** A comprehensive dataset encompassing a wide range of two-phase (liquid-vapor) phase change phenomena in boiling, with a focus on bubble and flow dynamics. This dataset will be of great interest to the scientific machine learning and thermal science communities.

**Real-world Validation.** Validation against experimental data to ensure the datasets accuracy and reliability. This validation process enhances the dataset’s fidelity and establishes a strong connection between simulation and real-world phenomena.

**Diverse Downstream Tasks.** BubbleML is designed to facilitate diverse downstream tasks. To demonstrate the dataset’s potential, we provide two benchmark scenarios: optical flow for learning bubble dynamics and scientific machine learning using operator networks to learn temperature dynamics and estimate heatflux.

## 2 Related Work

**Scientific Machine Learning Datasets.** There have been several efforts to develop benchmark datasets for scientific machine learning tasks [50, 36, 45]. Notably, PDEBench [50] provides a collection of datasets for 11 PDEs commonly encountered in computational fluid dynamics. However, the existing datasets in PDEBench primarily focus on relatively simpler cases that capture single-phase physics. While they serve as a good starting point for developing and evaluating SciML algorithms, they lack the necessary variability to represent the range of behaviors and phenomena encountered in scientific applications. In addition, boundary conditions in scientific simulations play a crucial role in capturing

<sup>2</sup>Through Zenodo, a permanent DOI for the dataset 10.5281/zenodo.8039787

the dynamics of the underlying physical systems. The majority of datasets in PDEBench utilize periodic boundary conditions. Although some datasets incorporate Neumann or Dirichlet boundary conditions, none of them consider a combination of both which can limit their ability to model real-world scenarios accurately.

In contrast, BubbleML focuses on capturing the complex dynamics and physics associated with multi-phase phenomena, particularly in the context of phase change simulations. Unlike many existing datasets that predominantly utilize a single type of boundary condition, BubbleML incorporates a combination of Dirichlet and Neumann boundary conditions [47]. This inclusion enables researchers to explore and model scenarios where multiple boundary conditions coexist, enhancing the realism and applicability of the dataset. Moreover, the presence of “jump” conditions along the liquid-vapor interface adds an additional layer of complexity. These conditions arise due to surface tension effects and require careful modeling to accurately capture the interface behavior [7]. By incorporating such challenges, BubbleML provides a realistic and demanding testbed for ML models.

**Optical Flow Datasets.** Optical flow estimation, a classical ill-posed problem[4] in image processing, has witnessed a shift from traditional methods to data-driven deep learning approaches. Middlebury [3] is a dataset with dense ground truth for small displacements, while KITTI2015 [32] provides sparse ground truth for large displacements in real-world scenes. MPI-Sintel [6] offers synthetic data with very large displacements, up to 400 pixels per frame. However, these datasets are relatively small for training deep neural networks. FlyingChairs [12], a large synthetic dataset, contains around 22,000 image pairs generated by applying affine transformations to rendered chairs on random backgrounds. FlyingThings3D [31] is another large synthetic dataset with approximately 25,000 stereo frames of 3D objects on different backgrounds.

While these datasets have been instrumental in advancing data-driven optical flow methods, they primarily focus on rigid object motion in visual scenes and do not address the specific challenges posed by multi-phase simulations. Efforts have been made to capture non-rigid motion in nature, such as piece-wise rigid motions seen in animals [24]. In boiling, the non-rigid dynamics of bubbles and the motion of liquid-vapor interfaces play a crucial role in the distribution and transfer of thermal energy. The BubbleML dataset provides a unique opportunity to explore and develop optical flow algorithms tailored to such dynamics. Unlike existing datasets, it offers a diverse range of bubble behaviors, including merging, growing, splitting, and complex interactions (see Figure 1). As a result, BubbleML fills a gap by providing challenging scenarios that involve phase change dynamics. The ability to accurately predict and forecast bubble dynamics has practical implications in various fields.

### 3 BubbleML: A Multi-phase Multi-physics Dataset for ML

In this section, we start by introducing the preliminary concepts underlying the SciML learning problem and give insights into the types of simulations and PDEs involved in this domain. Then, we present an overview of the dataset pipeline along with its validation against real-world experiments.

#### 3.1 Preliminaries

A common application for SciML is the solution of *boundary value problems* (BVPs). BVPs are widely used to model various physical phenomena, including fluid dynamics, heat transfer, electromagnetics, and quantum mechanics [47, 46, 35, 18]. BVPs take the form:  $L[u(x)] = f(x), x \in \Omega$  and  $B[u(x)] = g(x), x \in \partial\Omega$ . The goal is to determine the vector-valued solution function,  $u$ .  $x$  is a point in the domain  $\Omega$  and may include a temporal component. The boundary of the domain is denoted as  $\partial\Omega$ . The governing equation is described by the PDE operator  $L$ , and the forcing function is denoted as  $f$ . The *boundary condition* (BC) is given by the boundary operator  $B$  and the boundary function  $g$ .  $B[u] = g$  ensures the existence and uniqueness of the solution.

There are three common types of BCs: periodic, Dirichlet, and Neumann. Periodic BCs enforce the equality of the solution at distinct points in the domain:  $u(x_1) = u(x_2)$ . Dirichlet BCs specify the values of the solution on the boundary:  $u(x) = g(x)$ . Neumann BCs enforce constraints on the partial derivatives of the solution:  $\partial_{x_i} u(x) = g(x)$  [47]. As seen in Figure 1, BubbleML combines both Dirichlet (no-slip walls, heater, inflow) and Neumann (outflow) boundaries, which impose constraints on flow and temperature dynamics. Additionally, the “jump conditions” that govern the transitions between the liquid and vapor phases use Dirichlet and Neumann boundaries [7] [10].

#### 3.2 Overview of PDEs and Flash-X Simulation

A comprehensive description of the simulations is well beyond the scope of this paper and can be found in [10, 11]. We provide a concise description here as knowledge of the PDEs is important when training physics-informed models.

The liquid ( $l$ ) and vapor ( $v$ ) phases of a boiling simulation are characterized by differences in fluid and thermal properties: density,  $\rho$ ; viscosity,  $\mu$ ; thermal diffusivity,  $\alpha$ ; and thermal conductivity  $k$ . The phases are tracked using a level-set function,  $\phi$ , which is positive inside the vapor and negative in the liquid.  $\phi = 0$  provides implicit representation of the liquid-vapor interface,  $\Gamma$  (see Figure 1). The transport equations are non-dimensionalized and scaled using the values in liquid and are given as,

$$\frac{\partial \vec{u}}{\partial t} + \vec{u} \cdot \nabla \vec{u} = -\frac{1}{\rho'} \nabla P + \nabla \cdot \left[ \frac{\mu'}{\rho'} \frac{1}{\text{Re}} \nabla \vec{u} \right] + \frac{\vec{g}}{\text{Fr}^2} + \vec{S}_u^\Gamma + S_P^\Gamma \quad (1a)$$

$$\frac{\partial T}{\partial t} + \vec{u} \cdot \nabla T = \nabla \cdot \left[ \frac{\alpha'}{\text{Re Pr}} \nabla T \right] + S_T^\Gamma \quad (1b)$$

where,  $\vec{u}$ , is the velocity,  $P$  is the pressure, and  $T$  is the temperature everywhere in the domain. The Reynolds number (Re), Froude number (Fr), and Prandtl Number (Pr) are constants set for each simulation. Scaled fluid properties like,  $\rho'$ , represent the local value of the phase scaled by the corresponding value in liquid. Therefore,  $\rho'$  is 1 in liquid phase, and  $\rho_v/\rho_l$  for vapor phase. The effect of surface tension is modeled using Weber number (We) and incorporated by a sharp pressure jump,  $S_P^\Gamma$ , at the liquid-vapor interface,  $\Gamma$ . The effects of evaporation and saturation conditions on velocity and temperature,  $\vec{S}_u^\Gamma$ , and  $S_T^\Gamma$ , are modeled using a ghost fluid method [10]. For a more detailed discussion of non-dimensional parameters and values, we refer the reader to Appendix C.

The continuity equation is given by,  $\nabla \cdot \vec{u} = -\dot{m} \nabla(\rho')^{-1} \cdot \vec{n}$ , where the mass transfer  $\dot{m}$  is computed using local temperature gradients in liquid and vapor phase,  $\dot{m} = \text{St}(\text{Re Pr})^{-1} [\nabla T_l \cdot \vec{n}^\Gamma - k' \nabla T_v \cdot \vec{n}^\Gamma]$  where,  $\vec{n}^\Gamma$  is the surface normal vector to the liquid-vapor interface. The Stefan number St, is another constant defined for the simulation and depends on the the temperature scaling given by,  $\Delta T = T_{wall} - T_{bulk}$ , and latent heat of evaporation,  $h_{lv}$ . Simulation data is scaled to dimensional values using the characteristic length  $l_0$ , velocity  $u_0$ , and temperature  $(T - T_{bulk})/\Delta T$  scale. Temporal integration is implemented using a fractional step predictor-corrector formulation to enforce incompressible flow constraints. The solver has been extensively validated and demonstrates an overall second-order accuracy in space [10, 7, 11].

An important concept in thermal science is the heat flux,  $\bar{q}$ , which provides a metric for the efficiency of the boiling process. Heat flux is typically measured as the integral of gradient of temperature,  $\partial T/\partial y$ , over time and space at the heater surface. It includes contribution from various sub-processes related to conduction, convection, microlayer evaporation, and bubble induced turbulence. Identifying contribution from each sub-process and managing its behavior to improve the value of  $\bar{q}$  remains a challenge in this field[14].

The simulations in this study are implemented within the Flash-X framework [13, 10], and a dedicated environment is provided for running new simulations<sup>3</sup>. The repository contains example configuration files for various multiphase simulations, including those used in this dataset. To ensure reproducibility, a lab network has been designed that organizes each study using configuration files for data curation [9]. The lab notebook and Flash-X source code are open-source to allow for community development and contribution, enabling creation of new datasets beyond the scope of this paper. The simulation archives store HDF5 output files and bash scripts that document software environment and repository tags for reproducibility. The lab notebook also provides an option to package Flash-X simulations as standalone Docker/Singularity containers which can be deployed on cloud and supercomputing platforms without the need for installing third-party software dependencies. The latter is ongoing work towards software sustainability [51].

### 3.3 Dataset Overview

The study encompasses two types of boiling namely, pool boiling and flow boiling. Pool boiling represents fluid confined in a tank above a heater, resembling scenarios like cooling nuclear waste. The BCs for pool boiling include walls on the left and right, an outlet at the top, and a heater at the bottom. In contrast, flow Boiling models water flowing through a channel with a heater, simulating liquid cooling of data center GPUs. There is an inlet BC modeling flow into the system and an outlet. The fluid used for the simulations is FC-72 (perfluorohexane), an electrically insulating and stable fluorocarbon-based fluid commonly used for cooling applications in electronics operating at low temperatures (ranging from 50°C to 100°C). To explore various phenomena, different parameters such as heater temperature, liquid temperature, inlet velocity, and gravity scale are adjusted in each simulation. A summary of the dataset is presented in Table 1. Appendix D provides detailed illustrations of the boundary conditions and descriptions of each simulation for reference.

BubbleML stores simulation output in HDF5 files. Each HDF5 file corresponds to the state of a simulation at a specific instant in time and can be directly loaded into popular tensor types (e.g., PyTorch tensors or NumPy arrays)

<sup>3</sup> <https://anl.app.box.com/folder/214761430800?s=9fkwiocyxhgr1dyoxeg5j3mv571r0ec7h>

Table 1: Summary of BubbleML datasets with their respective spatial and temporal resolutions. 1 timestep corresponds to 1 second wall time. PB: Pool Boiling. FB: Flow Boiling

Dimensions	Type	Study	Sims	Resolution	Domain ( $mm^d$ )	Timesteps
2D	PB	Single Bubble	1	192 x 288	4.2 x 6.3	500
2D	PB	Saturated	13	512 x 512	11.2 x 11.2	200
2D	PB	Subcooled	10	384 x 384	8.4 x 8.4	200
2D	PB	Gravity	9	512 x 512	11.2 x 11.2	200
2D	FB	Inlet Velocity	8	1344 x 160	29.4 x 3.5	200
2D	FB	Gravity	6	1600 x 160	35 x 3.5	200
3D	FB	Gravity	4	400 x 400 x 400	8.75 x 8.75 x 8.75	50

using BoxKit. BoxKit is a custom Python API designed for efficient management and scalability of block-structured simulation datasets [53, 8]. It leverages multiprocessing and cache optimization techniques to improve read/write efficiency of data between disk and memory. Figure 2 provides an example of a boiling dataset and the corresponding workflow for enabling downstream tasks like scientific machine learning and optical flow. By operating on simulation data in manageable chunks that fit into memory, BoxKit significantly improves computational performance, particularly when handling large quantities of datasets.

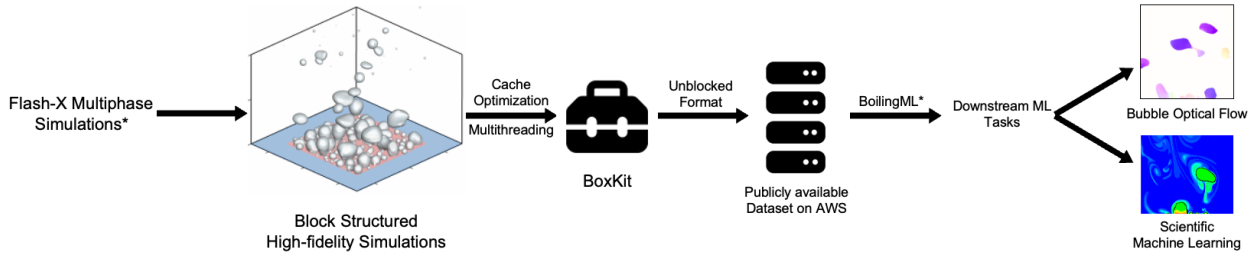


Figure 2: Dataset Curation and Workflow: Flash-X multiphase simulations are executed and converted into unblocked HDF5 formats using the BoxKit library. The resulting dataset is publicly available <sup>1</sup>, enabling downstream tasks like scientific machine learning and optical flow.

Each simulation within the BubbleML dataset tracks the velocities in the  $x$  and  $y$  directions, temperature, and a signed distance function (SDF),  $\phi$ , which represents the distance from the bubble interface. The SDF can be used to get a mask of the bubble interfaces or determine if a point is in the liquid or vapor phase. These variables are stored in HDF5 datasets. For instance, the temperature is stored in a tensor with a shape  $x \times y \times z \times t$ , which allows indexing with  $xyz$ -spatial coordinates or time. For 2D simulation datasets, the shape becomes  $x \times y \times t$ . The HDF5 files also include any constants or runtime parameters provided to the simulation. Some of these parameters, such as thermal conductivity or Reynolds number, are constants used in the PDEs that govern the system. The inclusion of these variables and parameters in the dataset enables comprehensive analysis and modeling of the boiling phenomena.

### 3.4 Dataset Validation

To ensure accuracy of scientific simulations, it is essential to validate them against experimental observations due to inherent approximations in numerical solvers and simplified models of real-world phenomena. Experimental findings [5] indicate that the heat flux increases linearly with the heater temperature until reaching the *Critical Heat Flux* (CHF), marking the transition from nucleate pool boiling to film boiling.

Figure 3 presents the bubble dynamics in two different regimes of saturated pool boiling: onset of nucleate boiling (ONB) and CHF. ONB occurs at low wall superheat and exhibits structured bubbly flow with consistent shape and size of departing bubbles from the heater surface. In contrast, the CHF regime is characterized by chaotic slug flow. Remarkably, the heat flux,  $\bar{q}$  at the heater surface for both sub-cooled and saturated boiling shown in Figure 3c closely match the experimental boiling curve, specifically for Si(100) surface [5]. Beyond CHF, the heat flux reaches a plateau, indicating a stasis marked by presence of large pockets of vapor cover on the heater surface as shown in Figure 3b.

Boiling is the most efficient mode of heat transfer on Earth and serves as a cooling mechanism for various thermal applications. However, in low gravity environments such as the International Space Station (ISS), the dynamics of bubble growth, merger, and departure, which significantly impact thermal efficiency, are influenced by the interplay

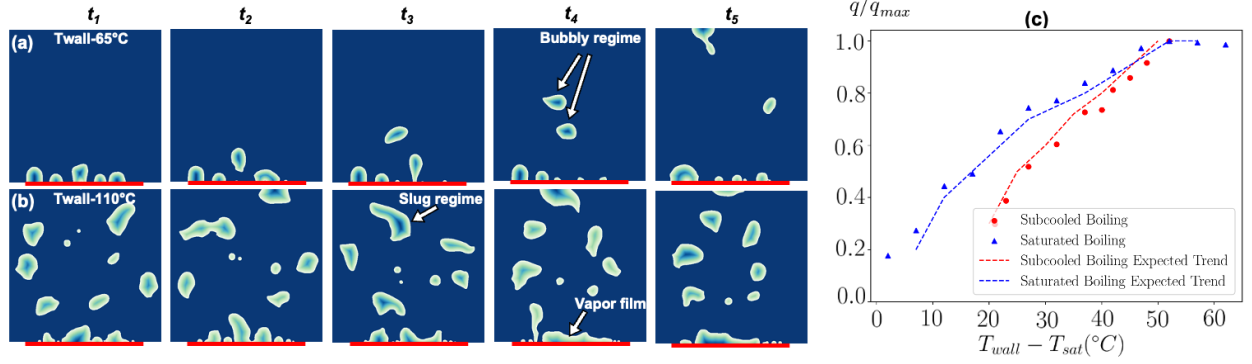


Figure 3: Bubble dynamics for saturated and subcooled pool boiling at different wall temperatures. (a) ONB during saturated boiling marked by a bubbly flow regime. (b) CHF behavior, indicated by the transition to slug flow. (c) Normalized heat flux,  $\bar{q}/\bar{q}_{max}$ , plotted against temperature difference between heater and liquid saturation temperature aligns with the boiling curve for FC-72.

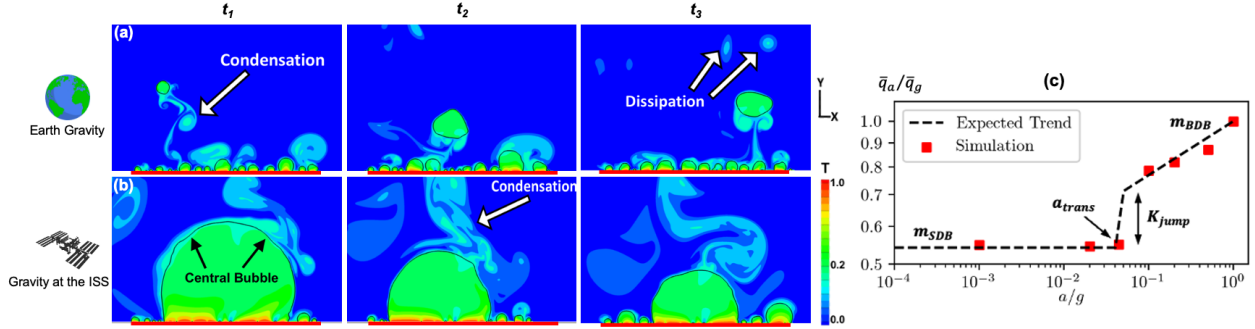


Figure 4: Gravity scaling of subcooled pool boiling: Bubble dynamics (black lines) and temperature distribution (contours) on (a) earth gravity,  $a/g = 1.0$ ,  $t_1 < t_2 < t_3$  and (b) low gravity,  $a/g = 0.001$ . (c) Wall heat flux vs. gravity for 2D simulations and its comparison to the scaling model in [39].

between surface tension and gravity. Quantifying these effects is crucial for developing phase change heat transfer systems in such environments.

Figure 4 provides an overview of simulations that were conducted to compare against the gravity-based heat flux model proposed in [39, 38]. These simulations cover a range of gravity levels,  $Fr = 1 - 100$ . The gravity scaling,  $a/g = \frac{1}{Fr^2}$ , is used to scale values relative to the Earth gravity ( $g$ ). Gravity separates pool boiling into two distinct regimes: buoyancy dominated boiling (BDB) and surface tension dominated boiling (SDB). The transitional acceleration,  $a_{trans}$ , which depends on the size of the heater, serves as the boundary between these two regimes.

In BDB, bubbles periodically detach from the heater surface when buoyancy takes over surface tension. Figure 4 illustrates the temporal evolution of temperature and the liquid-vapor interface during bubble departure events for  $a/g = 1$ . After departing from the surface, the bubbles undergo condensation due to subcooling, and generate vortices that gradually dissipate as they move upstream toward the outflow. This dissipation occurs as the vapor completely condenses into liquid. Decreasing gravitational acceleration results in larger departing bubbles and reduces the wall heat flux,  $\bar{q}$ . The scaling of  $\bar{q}$  with respect to gravity,  $\bar{q}_a/\bar{q}_g$ , follows the slope  $m_{BDB}$ . In SDB, the dynamics are dominated by the presence of a central bubble that remains on the heater surface and acts as a vapor sink for smaller satellite bubbles, as depicted in Figure 4 for  $a/g = 0.001$ . The figure also captures the transient behavior of the central bubble which fluctuates in size due to the balance between evaporation and condensation leading to different type of vortical structures. The heat flux drops sharply by a value  $K_{jump}$ , which depends on the size of the central bubble [11], and the slope,  $m_{SDB} = 0$ . The gravity scaling of heat flux computed from simulations accurately matches the expected trend from the model [38, 39], providing validation for the simulation results.

Table 2: Results of the RAFT and GMFlow models after training and fine-tuning on different combinations of datasets: FlyingChairs (C), FlyingThings3D (T), Sintel (S) and BubbleML (B)

Data	Method	Chairs(Val)	Things(Val)	Sintel(Train)		KITTI(Train)		Boiling(Test)
			Clean	Clean	Final	F1-EPE	F1-all	
C	RAFT	0.82	9.03	2.19	4.49	9.83	37.57	5.04
	GMFlow	0.92	10.23	3.22	4.43	17.82	56.14	5.61
C+B	RAFT	1.01	11.47	3.96	9.67	14.95	62.80	2.20
	GMFlow	1.57	12.66	4.01	5.28	22.52	63.80	1.82
C+T	RAFT	1.15	4.39	1.40	2.71	5.02	17.46	5.43
	GMFlow	1.26	3.48	1.50	2.96	11.60	35.62	9.42
C+T+B	RAFT	1.30	5.38	1.58	3.00	5.37	17.93	<b>1.57</b>
	GMFlow	1.39	3.97	1.80	3.12	16.33	49.11	<b>0.62</b>
C+T+S	RAFT	1.21	4.69	0.77	1.22	1.54	5.64	8.82
	GMFlow	1.53	4.09	0.95	1.28	3.04	13.61	20.05
C+T+S+B	RAFT	1.39	5.85	0.89	1.45	1.74	6.29	2.14
	GMFlow	1.66	4.5	1.09	1.47	4.03	19.77	3.07

## 4 Benchmarks of BubbleML: Optical Flow and SciML

### 4.1 Optical Flow

**Generation of Optical Flow Dataset.** Optical flow determines the velocity field of an image based on the relative movement of objects between consecutive frames. It has significant implications for downstream tasks such as extracting side-view boiling statistics and applying scientific machine learning to real world experimental data. BubbleML simulations provide an easy way to create an optical flow dataset for multiphase phenomena. Liquid-vapor phase distinction information from simulations is used to create image files where the bubbles are tracked between successive timesteps. The velocity data is then accessed for that particular timestep and the velocity of the liquid region is manually set to zero. This approach effectively ignores the fluid vortices and focuses solely on capturing the objects (bubbles) that are visible to the naked eye. The bubble velocities are then written to the widely accepted Middlebury [3] flow format, producing a sequence of images and flow files resembling the Sintel dataset[6]. To facilitate the training and validation of optical flow models, PyTorch dataloaders are provided for the generated dataset.<sup>45</sup> This allows for easy integration and fine-tuning of existing optical flow models using the BubbleML dataset.

**Benchmark.** For our benchmarks, we generate optical flow datasets for 6 different heater temperatures from our saturated boiling simulations and do a 80:20 training-validation split. This results in a boiling optical flow dataset (B) consisting of around 1000 training images and 200 validation images. We evaluate and fine-tune two state-of-the-art optical flow models, RAFT [52] and GMFlow [54], using this dataset. We consider three different pretrained models for each method: the first trained exclusively on FlyingChairs (C), the second trained on FlyingChairs and FlyingThings3D(C+T), and the third further fine-tuned on the Sintel(C+T+S). To assess the performance of the trained models, we measure the end-point error and summarize the results in Table 2.

Initially, we observe poor performance of these pretrained models on BubbleML. To address this, each model is fine-tuned for 3-4 epochs using the training data and a low learning rate of  $10^{-6}$ . After fine-tuning, we observe a significant improvement in predictions for the validation data, particularly for the bubble regions (see Appendix A Figure 6). It is worth noting that although training the models on the boiling dataset for more epochs improves performance on our specific task, it adversely affects the models’ generalization capabilities, leading to increased errors on other datasets. These findings highlight the effectiveness of fine-tuning the optical flow models on our boiling dataset.

### 4.2 Scientific Machine Learning

**SciML Preliminaries.** Our SciML experiments in BubbleML use **operator networks**, which is capable of learning the underlying PDE operator from ground truth training data. Operator networks offer the advantage of generalizing to domains with different BCs [26, 23] and can be used to perform new simulations. Specifically, we employ the auto-regressive formulation of a forward propagator operator, denoted as  $F$ , which maps the solution function  $u$  of  $k$  prior time steps  $t - k, \dots, t - 1$  to the solution at time  $t$ . Concisely,  $u([t - k, t - 1]) = u(t - k), \dots, u(t - 1)$ . The

<sup>4</sup><https://github.com/HPCForge/RAFT>

<sup>5</sup><https://github.com/HPCForge/gmflow>



operator  $F$  can be approximated using a neural network  $\mathcal{F}_\theta$  parameterized by  $\theta$ . This network is trained using a dataset of  $N$  ground truth solutions  $D = \{u^{(n)}(\cdot, [0, t_{max}]) : n = 1 \dots N\}$ . By applying a standard gradient descent algorithm, we find weights

$$\hat{\theta} = \arg \min_{\theta} \sum_{t=k}^{t_{max}} \sum_{n=1}^N \mathcal{L}[\mathcal{F}_\theta\{u^{(n)}(\cdot, [t-k, t-1])\}, u^{(n)}(\cdot, t)] \quad (2)$$

that minimize the loss function  $\mathcal{L}$  for the prediction and ground truth solutions. The trained model  $\mathcal{F}_{\hat{\theta}}$  can be applied to new problems by stepping through time. Given solutions for  $k$  initial timesteps, we can obtain an approximation  $\mathcal{F}_{\hat{\theta}}\{u(\cdot, [0, k-1])\} \approx u(\cdot, k)$ . Using this approximation, we can then approximate  $u(\cdot, k+1)$ , and the process is repeated until reaching  $t_{max}$ . In general, as it uses a series of approximations, errors may accumulate over time. Overall, operator networks offer a powerful framework for learning PDE operators and enable the application of trained models to simulate and approximate solutions for new time steps.

**Learning Temperature Dynamics.** We present an application of SciML using BubbleML, focusing on learning the dynamics of temperature propagation and flow when the velocities of a system are known. Such a model can be used to estimate the heatflux, as seen in Figure 5. We compare the performance of three commonly baseline models in SciML: 1. **U-Net** is a generic image-to-image architecture composed of convolutions with skip connections [40]. We modify the architecture to use the GELU activation function instead of Tanh [20]. 2. **Fourier Neural Operator (FNO)** applies weights in Fourier space. Unlike U-Net’s convolutions, FNO’s filters capture the global dynamics of the domain [26]. 3. **UNO** combines FNO’s Fourier blocks and mimics U-Net’s skip connections [23].

To evaluate the performance of these models, we take inspiration from PDEBench and adopt a set of metrics that include the Root Mean Squared Error (RMSE), Max Error, Relative Error, Boundary RMSE (BRMSE), and low/mid/high Fourier errors [50]. These metrics provide a comprehensive view of the physical dynamics, which may be missed when using a data loss metric alone, such as Mean Squared Error (MSE). For instance, when predicting temperature, the max error is often very high due to the presence of boundaries between hot vapor and cool liquid. A one-pixel misalignment in the model’s prediction can cause the temperature to be the opposite extreme. RMSE would not capture this, but such errors can have a large influence on heatflux calculations.

We propose an additional *physics* metric: the RMSE along bubble interfaces (IRMSE). The error along the domain boundary and bubble interfaces is very important. The boundary conditions determine if the solution to a PDE exists and is unique. In the case of the multi-physics BubbleML dataset, the jump conditions applied at the interface between the liquid and vapor phases must be satisfied.

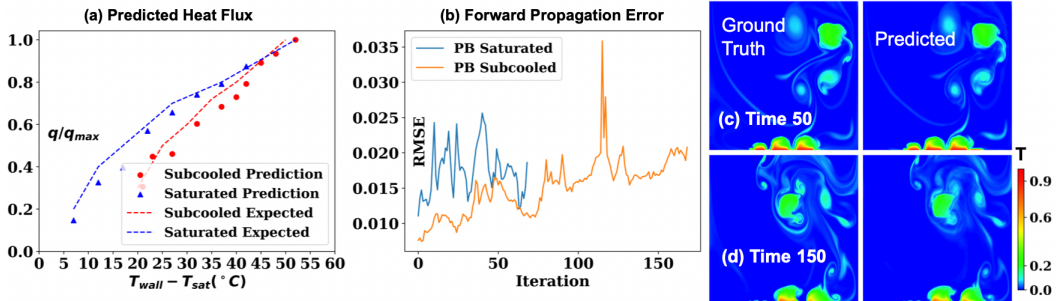


Figure 5: (a) Cross-validated heatflux  $q/q_{max}$  estimates for subcooled and saturated boiling. (b), (c), and (d) show results for the fully trained forward propagator. In (b), accuracy degradation is minimal, with spikes occurring during timesteps of violent turbulence caused by rapid bubble detachment from the heater surface. (c) and (d) compare frames from the Flash-X simulation and predictions by the forward propagator for subcooled boiling.

For each model, we follow the same training procedure as FNO [26]. We use the AdamW optimizer[27] and train each model for 500 epochs. The initial learning rate is set to  $1 \times 10^{-3}$  and is halved every 100 epochs. We train on the full resolution for each dataset. Figure 5 compares the predictions of the U-Net forward propagator (which was the best performing model) with the simulation ground truth. For a detailed comparison against all models, refer to Tables 3 and 4 in Appendix B.

To further validate our models, we performed cross-validation to predict the heatflux trends observed in Figure 3. For each heat flux prediction, we holdout that simulation and train a forward propagator on the remaining simulations in the dataset. Even with partial training—50 epochs for subcooled boiling models and 100 epochs for saturated boiling models—we achieved highly satisfactory results. The heatflux predictions remarkably track the expected trend, as seen

in Figure 5. These promising results indicate that our model effectively captures the underlying patterns in the data, despite the reduced training duration. Further training is expected to lead to improved heatflux estimates.

## 5 Conclusions

This paper presents the BubbleML dataset, which fills a critical gap in ML research for multiphase multiphysics systems. By employing physics-driven simulations, the dataset offers precise ground truth information for a variety of boiling scenarios, encompassing a wide range of parameters and providing a comprehensive and diverse collection of data. BubbleML is validated against experimental observations and trends, establishing its reliability and relevance in multi-physics phase change research. The two benchmark tasks demonstrate its application in improving the accuracy of optical flow estimation and hidden flow prediction in multiphase systems.

## 6 Acknowledgement

This work was partially supported by the National Science Foundation (NSF) under the award number 1750549, the Office of Naval Research (ONR) under grant number N00014-22-1-2063 (supervised by program manager Dr. Mark Spector), the Exascale Computing Project (17-SC-20-SC), a collaborative effort of the US Department of Energy Office of Science and the National Nuclear Security Administration, and Laboratory Directed Research and Development Program at Argonne National Lab, Office of Science, of the U.S. Department of Energy under Contract No. DE-AC02-06CH11357. We gratefully acknowledge the GPU computing resources provided on HPC3, a high-performance computing cluster operated by the Research Cyberinfrastructure Center at the University of California, Irvine.

## References

- [1] Amir Ali. Spreaders for immersion nucleate boiling cooling of a computer chip with a central hot spot. *Energy Conversion and Management*, 2012.
- [2] Daniel Attinger, Christophe Frankiewicz, Amy R Betz, Thomas M Schutzius, Ranjan Ganguly, Arindam Das, Chang-Jin Kim, and Constantine M Megaridis. Surface engineering for phase change heat transfer: A review. *MRS Energy & Sustainability*, 1:E4, 2014.
- [3] Simon Baker, Stefan Roth, Daniel Scharstein, Michael J. Black, J.P. Lewis, and Richard Szeliski. A database and evaluation methodology for optical flow. In *2007 IEEE 11th International Conference on Computer Vision*, pages 1–8, 2007.
- [4] S. S. Beauchemin and J. L. Barron. The computation of optical flow. *ACM Comput. Surv.*, 27(3):433–466, sep 1995.
- [5] Bradley Bon, James Klausner, and Edward McKenna. An investigation of pool boiling heat transfer on single crystal surfaces and a dense array of cylindrical cavities. *Journal of Heat Transfer*, 135, 09 2013.
- [6] Daniel J. Butler, Jonas Wulff, Garrett B. Stanley, and Michael J. Black. A naturalistic open source movie for optical flow evaluation. In Andrew Fitzgibbon, Svetlana Lazebnik, Pietro Perona, Yoichi Sato, and Cordelia Schmid, editors, *Computer Vision – ECCV 2012*, pages 611–625, Berlin, Heidelberg, 2012. Springer Berlin Heidelberg.
- [7] Akash Dhruv. *A Multiphase Solver for High-Fidelity Phase-Change Simulations over Complex Geometries*. PhD thesis, George Washington University, 2021.
- [8] Akash Dhruv. [github/akashdhruv/BoxKit](https://github.com/akashdhruv/BoxKit): October 2022, October 2022.
- [9] Akash Dhruv. [github/akashdhruv/Multiphase-Simulations](https://github.com/akashdhruv/Multiphase-Simulations): June 2023, 2023.
- [10] Akash Dhruv, Elias Balaras, Amir Riaz, and Jungho Kim. A formulation for high-fidelity simulations of pool boiling in low gravity. *International Journal of Multiphase Flow*, 120:103099, 2019.
- [11] Akash Dhruv, Elias Balaras, Amir Riaz, and Jungho Kim. An investigation of the gravity effects on pool boiling heat transfer via high-fidelity simulations. *International Journal of Heat and Mass Transfer*, 180:121826, 2021.
- [12] Alexey Dosovitskiy, Philipp Fischer, Eddy Ilg, Philip Hausser, Caner Hazirbas, Vladimir Golkov, Patrick Van Der Smagt, Daniel Cremers, and Thomas Brox. FlowNet: Learning optical flow with convolutional networks. In *Proceedings of the IEEE international conference on computer vision*, pages 2758–2766, 2015.
- [13] Anshu Dubey, Klaus Weide, Jared O’Neal, Akash Dhruv, Sean Couch, J. Austin Harris, Tom Klosterman, Rajeev Jain, Johann Rudi, Bronson Messer, Michael Pajkos, Jared Carlson, Ran Chu, Mohamed Wahib, Saurabh Chawdhary, Paul M. Ricker, Dongwook Lee, Katie Antypas, Katherine M. Riley, Christopher Daley, Murali

- Ganapathy, Francis X. Timmes, Dean M. Townsley, Marcos Vanella, John Bachan, Paul M. Rich, Shravan Kumar, Eirik Endeve, W. Raphael Hix, Anthony Mezzacappa, and Thomas Papatheodore. Flash-X: A multiphysics simulation software instrument. *SoftwareX*, 19:101168, 2022.
- [14] MA Ebadian and CX Lin. A review of high-heat-flux heat removal technologies. *Journal of heat transfer*, 133(11), 2011.
- [15] VM Efremenkov. Radioactive waste management at nuclear power plants. *Iaea Bulletin*, 31(4):37–42, 1989.
- [16] Frédéric Gibou, Liguo Chen, Duc Nguyen, and Sanjoy Banerjee. A level set based sharp interface method for the multiphase incompressible Navier-Stokes equations with phase change. *Journal of Computational Physics*, 222(2):536–555, 2007.
- [17] Jayesh K Gupta and Johannes Brandstetter. Towards multi-spatiotemporal-scale generalized pde modeling. *arXiv preprint arXiv:2209.15616*, 2022.
- [18] B. L. J. Gysen, K. J. Meessen, J. J. H. Paulides, and E. A. Lomonova. General formulation of the electromagnetic field distribution in machines and devices using fourier analysis. *IEEE Transactions on Magnetics*, 46(1):39–52, 2010.
- [19] Bassem M. Hamieh, James R. Beckman, and Michael D. Ybarra. Brackish and seawater desalination using a 20 ft<sup>2</sup> dewvaporation tower. *Desalination*, 140(3):217–226, 2001.
- [20] Dan Hendrycks and Kevin Gimpel. Gaussian error linear units (gelus), 2023.
- [21] Gustavo M Hobold and Alexandre K da Silva. Machine learning classification of boiling regimes with low speed, direct and indirect visualization. *International Journal of Heat and Mass Transfer*, 125:1296–1309, 2018.
- [22] Matthew T Hughes, Girish Kini, and Srinivas Garimella. Status, challenges, and potential for machine learning in understanding and applying heat transfer phenomena. *Journal of Heat Transfer*, 143(12), 2021.
- [23] Nikola B. Kovachki, Zongyi Li, Burigede Liu, Kamyar Azizzadenesheli, Kaushik Bhattacharya, Andrew M. Stuart, and Anima Anandkumar. Neural operator: Learning maps between function spaces. *CoRR*, abs/2108.08481, 2021.
- [24] Hoang-An Le, Tushar Nimbhorkar, Thomas Mensink, Sezer Karaoglu, Anil S. Baslamisli, and Theo Gevers. Unsupervised generation of optical flow datasets for videos in the wild, 2018.
- [25] Jonggyu Lee, Youngjoon Suh, Max Kuciej, Peter Simadiris, Michael T Barako, and Yoonjin Won. Computer vision-assisted investigation of boiling heat transfer on segmented nanowires with vertical wettability. *Nanoscale*, 14(36):13078–13089, 2022.
- [26] Zongyi Li, Nikola Kovachki, Kamyar Azizzadenesheli, Burigede Liu, Kaushik Bhattacharya, Andrew Stuart, and Anima Anandkumar. Fourier neural operator for parametric partial differential equations, 2020.
- [27] Ilya Loshchilov and Frank Hutter. Decoupled weight decay regularization, 2019.
- [28] Lu Lu, Pangzhan Jin, Guofei Pang, Zhongqiang Zhang, and George Em Karniadakis. Learning nonlinear operators via deepnet based on the universal approximation theorem of operators. *Nature Machine Intelligence*, 3:218–229, 2021.
- [29] Lu Lu, Xuhui Meng, Shengze Cai, Zhiping Mao, Somdatta Goswami, Zhongqiang Zhang, and George Em Karniadakis. A comprehensive and fair comparison of two neural operators (with practical extensions) based on fair data. *Computer Methods in Applied Mechanics and Engineering*, 393:114778, 2022.
- [30] Ziping Mao, Ameya D. Jagtap, and George Em Karniadakis. Physics-informed neural networks for high-speed flows. *Computer Methods in Applied Mechanics and Engineering*, 2020.
- [31] Nikolaus Mayer, Eddy Ilg, Philip Hausser, Philipp Fischer, Daniel Cremers, Alexey Dosovitskiy, and Thomas Brox. A large dataset to train convolutional networks for disparity, optical flow, and scene flow estimation. In *Proceedings of the IEEE conference on computer vision and pattern recognition*, pages 4040–4048, 2016.
- [32] Moritz Menze, Christian Heipke, and Andreas Geiger. Joint 3d estimation of vehicles and scene flow. *ISPRS annals of the photogrammetry, remote sensing and spatial information sciences*, 2:427, 2015.
- [33] I. Mudawar. Direct-immersion cooling for high power electronic chips. *[1992 Proceedings] Intersociety Conference on Thermal Phenomena in Electronic Systems*, 1992.
- [34] Mahdi Nabil and Alexander S Rattner. interthermalphasechange foam—a framework for two-phase flow simulations with thermally driven phase change. *SoftwareX*, 5:216–226, 2016.
- [35] Joseph Oliger and Arne Sundström. Theoretical and practical aspects of some initial boundary value problems in fluid dynamics. *SIAM Journal on Applied Mathematics*, 35(3):419–446, 1978.

- [36] Karl Otness, Arvi Gjoka, Joan Bruna, Daniele Panozzo, Benjamin Peherstorfer, Teseo Schneider, and Denis Zorin. An extensible benchmark suite for learning to simulate physical systems. In *35th Conference on Neural Information Processing Systems (NeurIPS 2021) Track on Datasets and Benchmarks*, 2021.
- [37] Maziar Raissi, Alireza Yazdani, and George Em Karniadakis. Hidden fluid mechanics: Learning velocity and pressure fields from flow visualizations. *Science*, 367(6481):1026–1030, 2020.
- [38] Rishi Raj, Jungho Kim, and John McQuillen. On the scaling of pool boiling heat flux with gravity and heater size. *Journal of Heat Transfer*, 134(1), Nov 2011. 011502.
- [39] Rishi Raj, Jungho Kim, and John McQuillen. Pool Boiling Heat Transfer on the International Space Station: Experimental Results and Model Verification. *Journal of Heat Transfer*, 134(10):101504, 2012.
- [40] Olaf Ronneberger, Philipp Fischer, and Thomas Brox. U-net: Convolutional networks for biomedical image segmentation. *Medical Image Computing and Computer-Assisted Intervention – MICCAI 2015*, pages 234–241, 2015.
- [41] Yohei Sato and Bojan Niceno. Pool boiling simulation using an interface tracking method: From nucleate boiling to film boiling regime through critical heat flux. *International Journal of Heat and Mass Transfer*, 125:876 – 890, 2018.
- [42] Yohei Sato and Bojan Ničeno. A sharp-interface phase change model for a mass-conservative interface tracking method. *Journal of Computational Physics*, 249:127 – 161, 2013.
- [43] Gihun Son and Vijay K. Dhir. A Level Set Method for Analysis of Film Boiling on an Immersed Solid Surface. *Numerical Heat Transfer, Part B: Fundamentals*, 52(January 2015):153–177, 2007.
- [44] Gihun Son and Vijay K. Dhir. Numerical simulation of nucleate boiling on a horizontal surface at high heat fluxes. *International Journal of Heat and Mass Transfer*, 51(9-10):2566–2582, 2008.
- [45] Kimberly L. Stachenfeld, Drummond B. Fielding, Dmitrii Kochkov, M. Cranmer, Tobias Pfaff, Jonathan Godwin, Can Cui, Shi-Lin Ho, Peter W. Battaglia, and Alvaro Sanchez-Gonzalez. Learned coarse models for efficient turbulence simulation. *ICLR*, 2022.
- [46] Ivar Stakgold. *Boundary Value Problems of Mathematical Physics: Volume 1*. SIAM, 2000.
- [47] Walter Strauss. *Partial Differential Equations An Introduction*. John Wiley & Sons, 2007.
- [48] Youngjoon Suh, Ramin Bostanabad, and Yoonjin Won. Deep learning predicts boiling heat transfer. *Scientific reports*, 11(1):1–10, 2021.
- [49] Youngjoon Suh, Jonggyu Lee, Peter Simadiris, Xiao Yan, Soumyadip Sett, Longnan Li, Kazi Fazle Rabbi, Nenad Miljkovic, and Yoonjin Won. A deep learning perspective on dropwise condensation. *Advanced Science*, 8(22):2101794, 2021.
- [50] Makoto Takamoto, Timothy Praditia, Raphael Leiteritz, Dan MacKinlay, Francesco Alesiani, Dirk Pflüger, and Mathias Niepert. PDEBench: An Extensive Benchmark for Scientific Machine Learning. In *36th Conference on Neural Information Processing Systems (NeurIPS 2022) Track on Datasets and Benchmarks*, 2022.
- [51] The Flash-X Team. [github/Flash-X/Workflows](https://github.com/Flash-X/Workflows): June 2023, 2023.
- [52] Zachary Teed and Jia Deng. Raft: Recurrent all-pairs field transforms for optical flow. 2020.
- [53] The HDF Group. Hierarchical data format version 5, 2000-2023.
- [54] Haofei Xu, Jing Zhang, Jianfei Cai, Hamid Rezatofighi, and Dacheng Tao. Gmflow: Learning optical flow via global matching. pages 8121–8130, 2022.
- [55] Miad Yazdani, Thomas Radcliff, Marios Soteriou, and Abbas A. Alahyari. A high-fidelity approach towards simulation of pool boiling. *Physics of Fluids*, 28(1):1–30, 2016.

## A Optical Flow

In this appendix we share qualitative results of Optical Flow models on BubbleML dataset. Figure 6 shows three sample pairs of input images, their ground truth optical flow and flow predictions from pretrained RAFT and GMFlow and their finetuned versions. It is observed that the optical flow predictions of the finetuned models improve significantly. Interestingly, it is observed that even though the performance of pretrained GMFlow models are worse than pretrained RAFT models, after finetuning GMFlow performs better than RAFT both quantitatively and qualitatively as seen in Table 2 and Figure 6.

**Compute Resources.** All models were finetuned using a single Nvidia V100 GPU. The implementations use the recommended versions of PyTorch and other libraries used in the official repositories of GMFlow and RAFT.

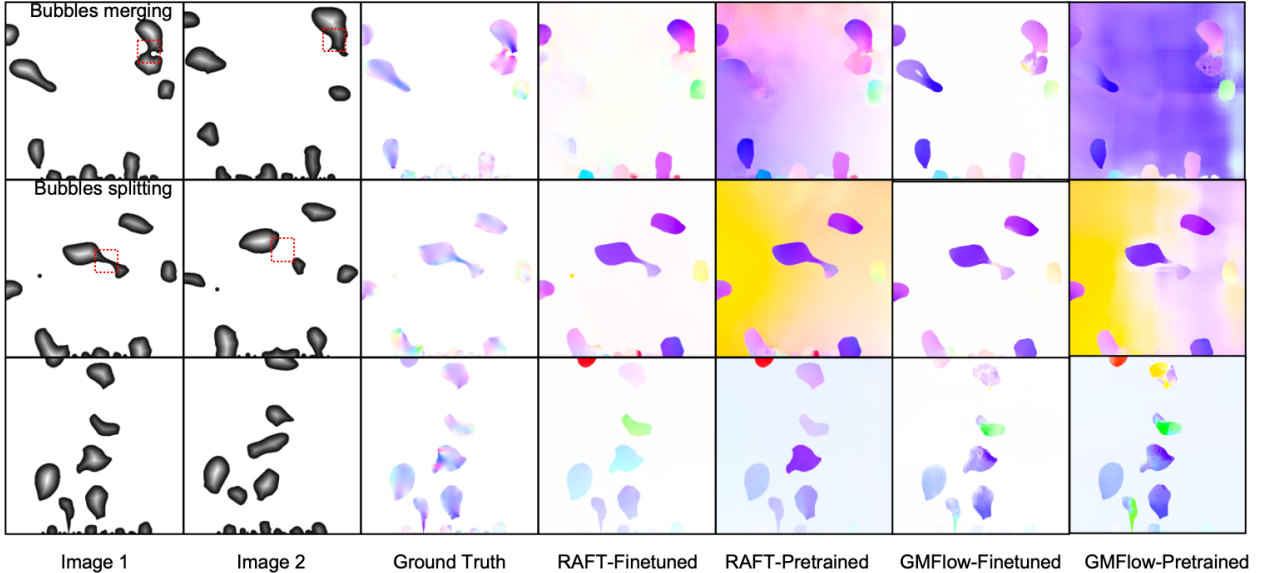


Figure 6: Comparison of pretrained Models with finetuned models on Pool Boiling Images

## B Scientific Machine Learning Results

In this appendix, we share a more complete listing of results for the Scientific Machine Learning sample applications.

**Pool Boiling.** Table 3 shows all of the metrics for each model on the pool boiling datasets. Interestingly, U-Net stands out as the best performing model across all metrics. The Fourier operator models (FNO and UNO) inherently assume some degree of periodicity, which is likely violated in our dataset due to non-periodic boundary conditions. FNO performs about an order of magnitude worse than U-Net on the BRMSE metric. Our findings align with recent literature comparing U-Net and FNO-based models. U-Net based PDE surrogates have demonstrated better interpolation and extrapolation performance compared to FNO and even hybrid architectures combining U-Net with FNO layers in its lower blocks [17]. Furthermore, FNO-like architectures seem highly susceptible to noise, resulting in their failure to predict solutions even with minimal Gaussian noise [29].

Another interesting metric is the Max Error. In general, this is high for every dataset because there is a fairly large gap in temperature between across the liquid-vapor interface: the liquid temperature is generally zero and the vapor sometimes gets up to one. The max error will be large when a model gets a “position” totally wrong and predicts a hot temperature for a very cold region. We can see that FNO and UNO struggle with this, getting a max error close to one on most datasets.

**Flow Boiling.** Figure 7 shows the forward propagator model applied to the Flow Boiling Gravity dataset. We can see that the model maintains high accuracy even after a large number of timesteps. This is because the inflow forces errors out of the viewing window, so the model frequently has a fresh start and errors do not accumulate as severely as the pool boiling datasets. Table 4 shows the metrics for each model applied to the flow boiling gravity dataset.

**Compute Resources.** All models were trained using a single Nvidia A30 GPU. The implementations use with PyTorch 2.0 running CUDA version 11.7.

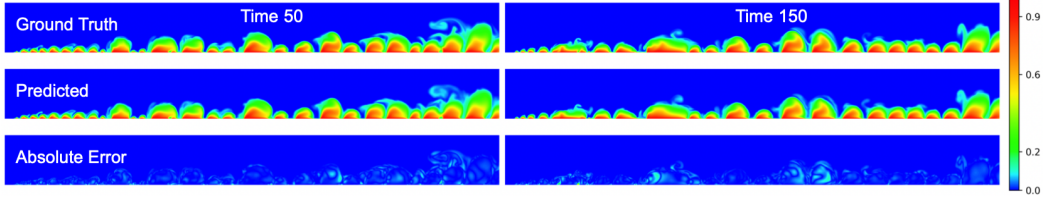


Figure 7: Sample output from applying forward propagating model to the Flow Boiling Gravity dataset. High accuracy can be maintained across many timesteps because the inflow forces everything (including incorrect predictions) out of frame.

Table 3: Pool Boiling Temperature Prediction

Dataset	Metric	U-Net	FNO	UNO
PB Saturated	Relative Error	0.25	0.93	0.52
	RMSE	$1.7 \times 10^{-2}$	$6.5 \times 10^{-2}$	$3.7 \times 10^{-2}$
	BRMSE	$5.3 \times 10^{-2}$	0.27	0.11
	IRMSE	$1.2 \times 10^{-2}$	$3.9 \times 10^{-2}$	$8.0 \times 10^{-2}$
	Max Error	0.91	0.98	0.99
	Fourier Low	0.14	0.64	0.23
	Fourier Mid	0.14	0.51	0.27
	Fourier High	$1.6 \times 10^{-2}$	$7.2 \times 10^{-2}$	$3.5 \times 10^{-2}$
PB Subcooled	Relative Error	0.18	0.79	0.34
	RMSE	$1.5 \times 10^{-2}$	$6.4 \times 10^{-2}$	$2.8 \times 10^{-2}$
	BRMSE	$7.0 \times 10^{-2}$	0.20	$6.2 \times 10^{-2}$
	IRMSE	$2.9 \times 10^{-2}$	0.11	$9.0 \times 10^{-2}$
	Max Error	0.79	1.00	0.69
	Fourier Low	0.10	0.78	0.21
	Fourier Mid	0.10	0.50	0.21
	Fourier High	$2.5 \times 10^{-2}$	$7.1 \times 10^{-2}$	$2.9 \times 10^{-2}$
PB Gravity	Relative Error	0.16	0.78	0.52
	RMSE	$1.6 \times 10^{-2}$	$8 \times 10^{-2}$	$5.4 \times 10^{-2}$
	BRMSE	$2.4 \times 10^{-2}$	0.24	0.22
	IRMSE	$2.2 \times 10^{-2}$	0.10	0.10
	Max Error	0.43	1.0	1.0
	Fourier Low	0.21	1.2	0.58
	Fourier Mid	0.11	0.61	0.33
	Fourier High	$1.2 \times 10^{-2}$	$7.7 \times 10^{-2}$	$8.1 \times 10^{-2}$

Table 4: Flow Boiling Temperature Prediction

Dataset	Metric	U-Net	FNO	UNO
FB Gravity	Relative Error	$6.2 \times 10^{-2}$	0.50	0.38
	RMSE	$1.4 \times 10^{-2}$	0.11	$8.4 \times 10^{-2}$
	BRMSE	$2.6 \times 10^{-2}$	0.19	0.16
	IRMSE	$1.7 \times 10^{-2}$	0.22	0.19
	Max Error	0.60	1.0	1.0
	Fourier Low	$7.2 \times 10^{-2}$	0.57	0.43
	Fourier Mid	$7.9 \times 10^{-2}$	0.62	0.43
	Fourier High	$4.0 \times 10^{-2}$	0.31	0.24

## C Physical and non-dimensional values

### C.1 Fluid properties

Table 5 provides a comprehensive list of physical properties relevant to multiphase flow. These properties are presented with their respective symbols, units, and descriptions. It is important to consider the properties of the liquid and vapor phases separately in multiphase flows, as they exhibit distinct characteristics due to the phase change phenomenon.

Additionally, the temperatures of the heater and liquid are also taken into account, as they significantly influence bubble dynamics and flow behaviors. The saturation temperature, which marks the initiation of bubble generation, is determined by the specific fluid being studied.

Table 5: Physical properties with symbol and unit

Symbol	Unit	Description
$\rho_l$	$kg/m^3$	Liquid density
$\rho_v$	$kg/m^3$	Vapor density
$\mu_l$	$N \cdot s/m^2$	Dynamic viscosity of liquid
$\mu_v$	$N \cdot s/m^2$	Dynamic viscosity of vapor
$C_{p,l}$	$J/kg \cdot K$	Specific heat capacity of liquid
$C_{p,v}$	$J/kg \cdot K$	Specific heat capacity of vapor
$k_l$	$W/m \cdot K$	Thermal conductivity of liquid
$k_v$	$W/m \cdot K$	Thermal conductivity of vapor
$h_{vl}$	$J/kg$	Latent heat
$g$	$m/s^2$	Gravitational acceleration
$\sigma$	$N/m$	Surface tension
$T_{wall}$	$K$	Heater temperature
$T_{bulk}$	$K$	Bulk temperature
$T_{sat}$	$K$	Saturation temperature

## C.2 Conversion to Non-dimensional parameters

Table 6 provides a comprehensive list of non-dimensional variables used in this study, including their symbols, definitions, and descriptions. These non-dimensional variables are necessary to solve the non-dimensionalized governing equations such as the continuity, momentum, and energy equations. Additionally, non-dimensional properties such as density, dynamic viscosity, specific heat capacity, and thermal conductivity are also considered in the context of multiphase flow. Notably, representative parameters in fluid mechanics, thermodynamics, and heat transfer, such as the Reynolds number ( $Re$ ), Froude number ( $Fr$ ), Prandtl number ( $Pr$ ), Stefan number ( $St$ ), Weber number ( $We$ ), and Peclet number ( $Pe$ ), are used to obtain simulation results. By employing non-dimensionalization, the effects of different physical quantities can be studied independently of their specific units, facilitating a deeper understanding of the underlying phenomena.

Table 6: Formulae used for conversion of real world values to non-dimensional values

Symbol	Definition	Description
$\rho^*$	$\rho_v/\rho_l$	Non-dimensional density
$\mu^*$	$\mu_v/\mu_l$	Non-dimensional viscosity
$C_p^*$	$C_{p,v}/C_{p,l}$	Non-dimensional specific heat capacity
$k^*$	$k_v/k_l$	Non-dimensional thermal conductivity
$l_0$	$\sqrt{\sigma/g\Delta\rho}$	Characteristic length scale
$u_0$	$\sqrt{gl_0}$	Characteristic velocity scale
$t_0$	$l_0/u_0$	Characteristic time scale
$T_{wall}^*$	$(T_{wall} - T_{bulk})/(T_{wall} - T_{bulk}) = 1$	Non-dimensional heater temperature
$T_{bulk}^*$	$(T_{bulk} - T_{bulk})/(T_{wall} - T_{bulk}) = 0$	Non-dimensional bulk temperature
$T_{sat}^*$	$(T_{sat} - T_{bulk})/(T_{wall} - T_{bulk})$	Non-dimensional saturated temperature
$Re$	$\rho_l u_0 l_0 / \mu_l$	Reynolds number
$Fr$	$u_0 / \sqrt{gl_0}$	Froude number
$Pr$	$\mu_l C_{p,l} / k_l$	Prandtl number
$St$	$C_{p,l} (T_{wall} - T_{bulk}) / h_{vl}$	Stefan number
$We$	$\rho_l u_0^2 l_0 / \sigma$	Weber number
$Pe$	$Re \cdot Pr$	Peclet number

## D Simulation Details

### D.1 Multiphase Simulations

Numerical simulations of multiphase flows with phase changes have been studied using various techniques to model the behavior at the liquid-vapor interface and track its evolution over time. Two commonly used methods for handling boundary conditions related to surface tension and evaporation are the ghost fluid method (GFM) and the continuum surface force method (CSF). The GFM enforces a sharp jump in pressure, velocity, and temperature across the interface, while the CSF diffuses the forcing within the vicinity of the interface for a smoother transition. The choice between these approaches involves a trade-off between accuracy and stability, with GFM offering higher accuracy but lower stability compared to CSF. Interface tracking is typically achieved implicitly using level-set or volume of fluid (VOF) techniques.

Researchers have employed these methods to study and model various aspects of multiphase flows with phase changes. For example, Gibou et al. [16] used a level-set method with sharp interfacial jump conditions within the framework of the GFM to model homogeneous two-dimensional evaporation and film boiling. Son and Dhir [43, 44] extended this approach to perform heterogeneous pool boiling calculations involving single and multiple bubbles. Majority of their initial work focused on model development and verification using two-dimensional (2D) simulations, since real world three-dimensional (3D) calculations were expensive due to limitations of the software framework.

Efforts have also been made to perform high-fidelity 3D simulations of pool boiling by combining different techniques. Yazadani et al. [55] conducted critical heat flux (CHF) calculations on earth gravity using a combination of VOF and CSF methods. Sato et al. [42, 41], on the other hand used the level-set method in combination with CSF for their simulations. These studies highlighted the computational cost associated with boiling simulations which had to be mitigated by performing low resolution calculations. More recently, Dhruv et al. [10, 11] used a combination of level-set and GFM methods for gravity scaling analysis of pool boiling at finer resolution than previous studies using adaptive mesh refinement (AMR) within the framework of FLASH. These simulations were applied to study effects of gravity on boiling heat transfer which lead to verification of experiment based heat flux models and enabled the quantification of turbulent heat flux associated with bubble dynamics during bubbly and slug flow [11]. The implementation of multiphase models within FLASH has transitioned to Flash-X, which leverages state-of-art AMR techniques and heterogeneous supercomputing architectures to significantly improve performance of boiling calculations. The BubbleML dataset is curated from simulations carried out with the Flash-X framework.

An important note is that simulations still heavily rely on experimental observations to determine input conditions such as nucleation site distribution, bubble nucleation frequency, and solid-liquid-vapor contact angle dynamics [10, 7]. As a result, simulations serve as an effective tool to understand and quantify trends in boiling regimes, rather than attempting to replicate experiments precisely. This opens up an opportunity for the integration of data-driven ML techniques, which can leverage diverse datasets to make informed predictions for boiling phenomena.

### D.2 Fluid parameters

The input configuration file of a simulation requires the inclusion of certain parameters, which remain constant for a specific fluid. For our simulations using FC-72 (Perfluorohexane,  $C_6F_{14}$ ), the non-dimensional values for this fluid are provided in Table 7. It is important to note that parameters corresponding to any specific real-world fluid must be converted to these non-dimensional values before being input into the simulation configuration files. This conversion allows for consistent and standardized representation of fluid properties in the simulation, enabling accurate and meaningful results to be obtained.

Table 7: Non-dimensional constants for FC-72, the fluid used in BubbleML

Parameter	Variable Name	Non-dimensional Value
Inverse Reynolds Number, $\frac{1}{Re}$	ins_invReynolds	0.0042
Non-dimensional density, $\rho^*$	mph_rhoGas	0.0083
Non-dimensional viscosity, $\mu^*$	mph_muGas	1.0
Non-dimensional thermal conductivity, $k^*$	mph_thcoGas	0.25
Non-dimensional specific heat capacity, $C_p^*$	mph_CpGas	0.83
Inverse Weber Number, $\frac{1}{We}$	mph_invWeber	1.0
Prandtl Number, $Pr$	ht_Prandtl	8.4